

Article

Structural, Magnetic and Vibrational Properties of Van Der Waals Ferromagnet CrBr₃ at High Pressure

Olga Lis ^{1,2} , Denis Kozlenko ¹, Sergey Kichanov ^{1,*} , Evgenii Lukin ¹, Ivan Zel ¹  and Boris Savenko ¹¹ Frank Laboratory of Neutron Physics, Joint Institute for Nuclear Research, 141980 Dubna, Russia² Department of Nuclear-Physical Materials Science, Institute of Physics, Kazan (Volga Region) Federal University, 420008 Kazan, Russia

* Correspondence: ekich@nf.jinr.ru

Abstract: The crystal and magnetic structures of van der Waals layered ferromagnet CrBr₃ were studied using X-ray powder diffraction and neutron powder diffraction at pressures up to 23 GPa at ambient temperature and up to 2.8 GPa in the temperature range 6–300 K, respectively. The vibration spectra of CrBr₃ were studied using Raman spectroscopy at pressures up to 23 GPa at ambient temperature. The anomalous pressure behavior of structural parameters and vibrational modes was observed, associated with a gradual isostructural phase transition in the pressure range 2.5–7 GPa. The Curie temperature T_C reduced rapidly with a pressure coefficient $dT_C/dP = -4.1(4)$ K/GPa. A full suppression of the ferromagnetic state was expected at $P_C \sim 8.4$ GPa, where onset of the antiferromagnetic spin arrangement or magnetically disordered state may take place. Anomalies in Raman spectra at $P \sim 15$ GPa point to another possible phase transformation in CrBr₃, which may be related to the proximity of metallization of this van der Waals ferromagnet.

Keywords: neutron diffraction; high pressure; crystal and magnetic structure; phase transition; van der Waals ferromagnet



Citation: Lis, O.; Kozlenko, D.; Kichanov, S.; Lukin, E.; Zel, I.; Savenko, B. Structural, Magnetic and Vibrational Properties of Van Der Waals Ferromagnet CrBr₃ at High Pressure. *Materials* **2023**, *16*, 454. <https://doi.org/10.3390/ma16010454>

Academic Editor: Vlassios Likodimos

Received: 8 December 2022

Revised: 29 December 2022

Accepted: 31 December 2022

Published: 3 January 2023



Copyright: © 2023 by the authors. Licensee MDPI, Basel, Switzerland. This article is an open access article distributed under the terms and conditions of the Creative Commons Attribution (CC BY) license (<https://creativecommons.org/licenses/by/4.0/>).

1. Introduction

A discovery of intrinsic ferromagnetism in two-dimensional (2D) atomically thin van der Waals (vdW) magnets initiated comprehensive fundamental and applied research of these materials, demonstrating challenging physical phenomena and highly promising for applications in spintronics and electronics [1–8]. The layered structure and the vdW gap between the layers in two-dimensional vdW magnets provide different routes to manipulate their magnetic properties. In particular, an application of high pressure through changing interatomic distances and angles gives an effective way to adjust both magnetic and electronic properties without changing the chemical composition [9,10]. Applying pressure predominantly compresses the weakly bonded interplanar distances and switches the lattice toward a 3D character in a van der Waals magnet. As an example, pressure causes changes in the stacking magnetic order of layers, which induces a phase transition from antiferromagnetic to ferromagnetic in the bilayer system CrI₃ [9–11].

Recent studies have demonstrated a rich variety of pressure-induced phenomena in vdW materials. In antiferromagnet FePX₃ (X = S, Se) pressure-induced insulator–metal transition, structural transitions, and spin crossover, and also the emergence of superconductivity (in FePSe₃), were reported [12–14]. In FePS₃, the initial antiferromagnetic interplanar coupling with strong 2D character is switched by high pressure to a ferromagnetic interplanar one and the magnetic state evolves from 2D-like to 3D-like character [15]. In CrSiTe₃, the ferromagnetically ordered state transfers to the paramagnetic one with increasing pressure, accompanied by a structural transition and the appearance of superconductivity [16]. In Cr₂Ge₂Te₆, pressure-induced spin reorientation was discovered, which drove equilibrium magnetization from the c axis to the ab plane [17]. The vdW ferromagnets demonstrate a different response of T_C under pressure. While it increases in CrI₃ and

VI₃ [18,19], a suppression of T_C was found in Cr₂Ge₂Te₆ [20], CrBr₃ [21], Fe₃GeTe₂ [22]. A pressure-induced semiconductor-to-metal transition was observed in CrI₃, accompanied by strengthening of the AFM interactions [23]. The isostructural phase transition in CrCl₃ was detected at about ~10 GPa, followed by electronic topological transition and metallization at P~30 GPa [24,25].

Among the vdW CrY₃ family (Y = Cl, Br, I), the structural and magnetic properties of the CrBr₃ representative remain weakly explored. Recently this material has attracted particular attention due to pronounced negative thermal expansion effects [26–28]. It crystallizes in a rhombohedral structure of $R\bar{3}$ symmetry, where the Cr atoms form a honeycomb lattice, which is clenched by two atomic planes of Br atoms. The ferromagnetic order is settled in CrBr₃ below the critical temperature of 36 K. In this work, the structural, magnetic and vibrational properties of CrBr₃ under high pressure were studied by a combination of X-ray, neutron diffraction and Raman spectroscopy techniques.

2. Materials and Methods

The polycrystalline CrBr₃ sample was made from single crystals supplied by HQ Graphene. The X-ray powder diffraction (XRD) experiments at high pressures up to 23 GPa were performed using the SAXS/WAXS Xeuss 3.0 system (XENOCOS SAS, Grenoble, France) with the Dectris Eiger 2R 1 M detector, Mo K_{α} radiation ($\lambda = 0.71078 \text{ \AA}$). The Almax Plate type diamond anvil cell was used. Diamonds with culets of 250 μm were taken. The sample was loaded into a hole of 150 μm diameter made in the Re gasket to about 20 μm thickness.

Neutron powder diffraction (ND) measurements were performed in the temperature range 6–300 K at pressures up to ~3 GPa using a DN-6 diffractometer [29] at IBR-2 high flux pulsed reactor (FLNP JINR, Dubna, Russia). A powder sample volume of about 2 mm² was loaded into the sapphire anvil high pressure cells [30]. The spherical holes with a diameter of 2 mm were drilled at the anvil's culets for the quasi-hydrostatic pressure distribution at the sample surface. Several tiny ruby chips were placed at different points of the sample surface and the pressure was determined by a standard ruby fluorescence technique. Measurements of the pressure distribution on the sample yielded typical pressure inhomogeneities of $\pm 15\%$. The diffraction patterns were collected at the scattering angle of 90° with a resolution of $\Delta d/d = 0.022$. The neutron and X-ray diffraction data were analyzed by the Rietveld method using the Fullprof 7.6 software [31].

Raman spectra at ambient temperature and pressures up to ~20 GPa were collected using a LabRAM HR spectrometer (Horiba Gr, Montpellier, France) with a wavelength excitation of 633 nm emitted from He–Ne laser, 1800 grating, a confocal hole of 100 μm , and $\times 20$ objective. The Almax Plate type diamond anvil cell was used.

3. Results

3.1. X-ray Diffraction

The XRD patterns of CrBr₃ measured at selected pressures and ambient temperature are shown in Figure 1a. They correspond to the initial rhombohedral crystal structure of $R\bar{3}$ symmetry. The values of lattice parameters determined at ambient conditions, $a = 6.270(4)$ and $c = 18.269(5) \text{ \AA}$, were consistent with those obtained previously [6,26,32]. At moderate pressures, the lattice compression of CrBr₃ was markedly anisotropic (Figure 1c) with the c lattice parameter nearly twice as compressible as the a parameter. The corresponding average compressibility values [$k_i = -(1/a_{i0})(da_i/dP)_T$] were $k_{a1} = 0.0067(3)$ and $k_{c1} = 0.0147(2) \text{ GPa}^{-1}$. At transition pressure $P_{tr} \sim 7 \text{ GPa}$, a significant change in pressure behavior of the c lattice parameter occurred (Figure 1c). Its compressibility was reduced by about four times to $k_{c2} = 0.0035(4) \text{ GPa}^{-1}$, becoming comparable with that of the a parameter, which decreased by more than twice to $k_{a2} = 0.0026(1) \text{ GPa}^{-1}$. In the absence of qualitative changes in the XRD patterns, one may suggest that the observed lattice compression anomaly was associated with the isostructural phase transition into a denser phase with reduced distance between the vdW layers. A somewhat similar phenomenon was also observed in a related compound CrCl₃ at ~11 GPa [25]. It should be noted that

the pressure-induced phase transition in CrY₃ materials occurred in a smoother manner in comparison with FePX₃ (X = S, Se) systems, where first-order structural phase transitions at ~13 GPa and ~8 GPa, respectively, were accompanied by discontinuous drops of the lattice parameters [12,14]. This observed large-volume collapse has been proposed to be associated with spin-crossover and insulator-metal transitions. It is also interesting to note that, in contrast to CrY₃, in ternary CrSiTe₃ and Cr₂Ge₂Te₆ systems, a pressure-induced suppression of the crystalline phase, followed by an amorphization process, was reported [33,34].

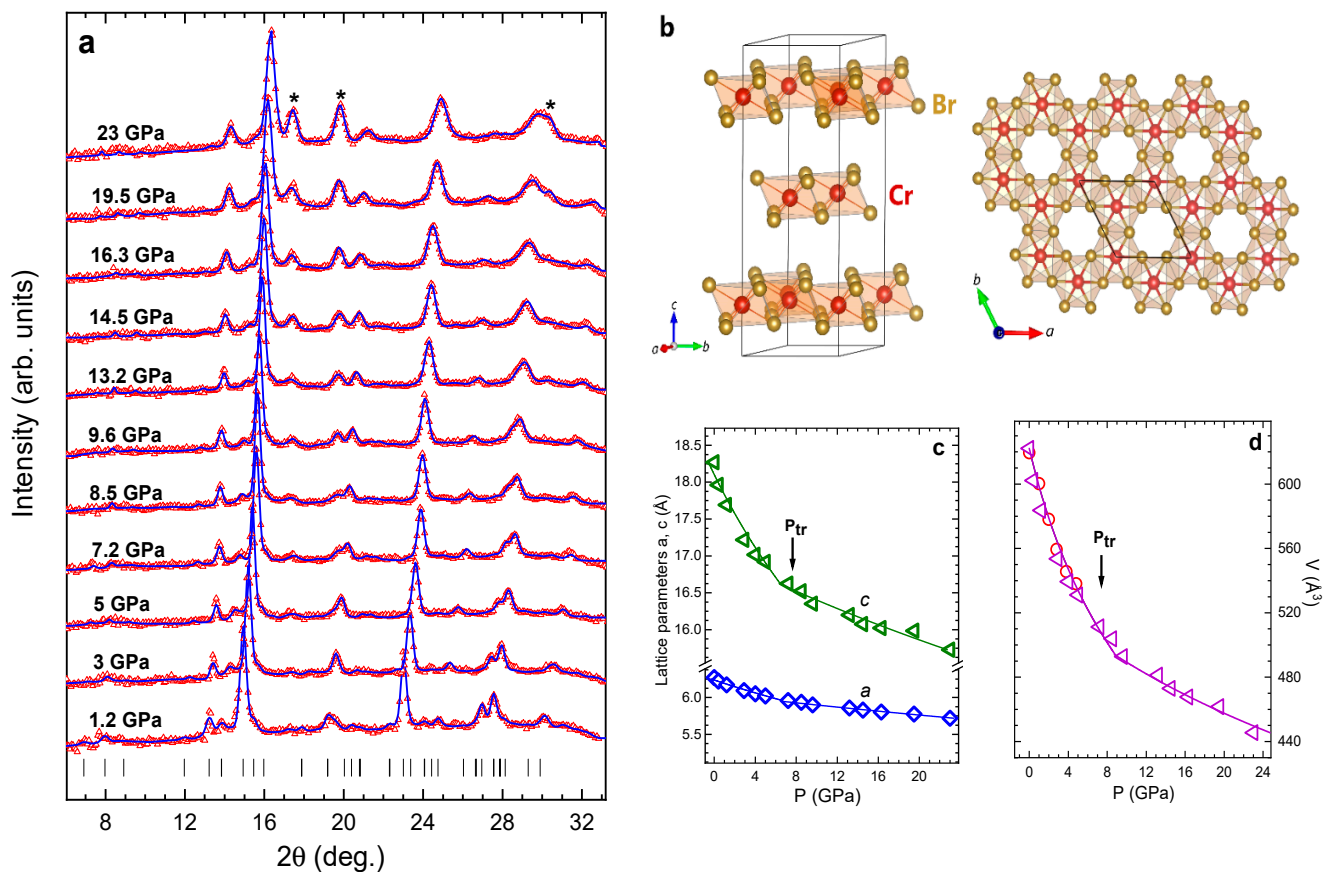


Figure 1. (a) X-ray diffraction patterns of CrBr₃ obtained at selected pressures and ambient temperature, and refined by the Rietveld method. Experimental points and calculated profiles are shown. The tick below marks the calculated positions of the structural peaks of phase of rhombohedral phase of CrBr₃. The asterisks (*) indicate additional diffraction peaks from the rhenium gasket; (b) Schematically representation of rhombohedral crystal structure of CrBr₃. The unit cell (left) and top view (right) are shown. The orientation of the crystallography axes is presented; (c) The lattice parameters of CrBr₃ as a function of pressure. The phase transition pressure P_{tr} is labeled. The solid lines are linear fit of experimental data; (d) The pressure dependence of unit cell volume of the ambient and high-pressure phases of CrBr₃, fitted by the third order Birch-Murnaghan equation of state (1). The red circles represent the obtained values for unit-cell volume from ND data (see below).

The volume compressibility data of CrBr₃ (Figure 1d) were fitted by the third-order Birch–Murnaghan equation of state (1) [35]:

$$P = \frac{3}{2}B_0 \left(x^{-7/3} - x^{-5/3} \right) \left[1 + \frac{3}{4}(B' - 4)(x^{-2/3} - 1) \right] \quad (1)$$

where $x = V/V_0$ is the relative volume change; V_0 is the unit cell volume at ambient pressure; B_0 , B' are the bulk modulus [$B_0 = -V(dP/dV)_T$] and its pressure derivative [$B' = (dB_0/dP)_T$].

The obtained bulk moduli for the ambient pressure and high-pressure phases were $B_0 = 23(4)$ and $B_0 = 94(3)$ GPa at fixed $B' = 4$. The ambient-pressure phase value was comparable with those obtained for CrCl_3 ($B_0 = 28(2)$ GPa) [25]; CrSiTe_3 ($B_0 \sim 37(1)$ GPa, $B' = 3.82$) [34]; and $\text{Cr}_2\text{Ge}_2\text{Te}_6$ ($B_0 = 39.2$ GPa, $B' = 3.8$) [36].

3.2. Neutron Diffraction

Neutron diffraction patterns of CrBr_3 , measured at selected pressures and temperatures, are shown in Figure 2. At ambient pressure below $T_C = 36(2)$ K, the appearance of additional magnetic contribution to intensities of the peaks (110), (012), (101) was revealed, indicating formation of the FM state [26]. The ordered magnetic moments were oriented along the c -axis and their values were $M = 2.74(8) \mu_B$. Remarkably, the strongly anisotropic thermal expansion of the CrBr_3 lattice with the pronounced variation of the c lattice parameter was also observed, even upon compression up to 2.8 GPa. As a result, the negative thermal expansion of the unit cell volume for $T < T_C$ was preserved in the studied pressure range (Figure 3a). This effect was associated with a strong spin–phonon coupling [26]. The average volume thermal expansion coefficients ($a_V = (1/V)(dV/dT)$) were $a_V = 2.2 \times 10^{-5} \text{ K}^{-1}$ for $T > T_C$ and $a_V = -1.8 \times 10^{-5} \text{ K}^{-1}$ for $T < T_C$ at $P = 1$ GPa and $a_V = 1.9 \times 10^{-5} \text{ K}^{-1}$ for $T > T_C$ and $a_V = -1.4 \cdot 10^{-5} \text{ K}^{-1}$ for $T < T_C$ at $P = 2$ GPa. The obtained coefficients for regions below T_C decreased with application of pressure, and this effect correlated with a suppression of long-range magnetic ordering, as we discuss below.

With a pressure increase, a progressive reduction of the magnetic contribution, to the (110) and (101) peaks, was detected (Figure 2), evidencing reduction of magnetic moment and suppression of magnetic ordering.

The temperature dependences of the Cr^{3+} magnetic moments at selected pressures are shown in Figure 3b. They were analyzed in the framework of the molecular field model using expression:

$$\frac{M}{M_0} = B_s \left(\frac{3S}{S+1} \frac{M}{M_0} \frac{T_C}{T} \right) \quad (2)$$

where B_s is the Brillouin function, S is the spin of the system ($S = 3/2$) and M_0 is the ordered magnetic moment at $T = 0$. The obtained Curie temperature decreased under pressure with a coefficient $dT_C/dP = -4.1(4)$ K/GPa (Figure 3c). Simultaneously, the ordered Cr^{3+} magnetic moments of the FM state at $T = 6$ K decreased from $2.74(8) \mu_B$ to $1.8(4) \mu_B$ in the pressure range 0–2.8 GPa. These decreasing trends were also detected for this compound earlier from magnetization measurements in a more restricted pressure range up to 1 GPa, providing a comparable value of $dT_C/dP = -3.1$ K/GPa [32]. The pressure behavior of CrBr_3 was opposite to CrI_3 , where a pronounced increase of T_C , by about 7.5%, for an applied pressure of 1 GPa occurred [18].

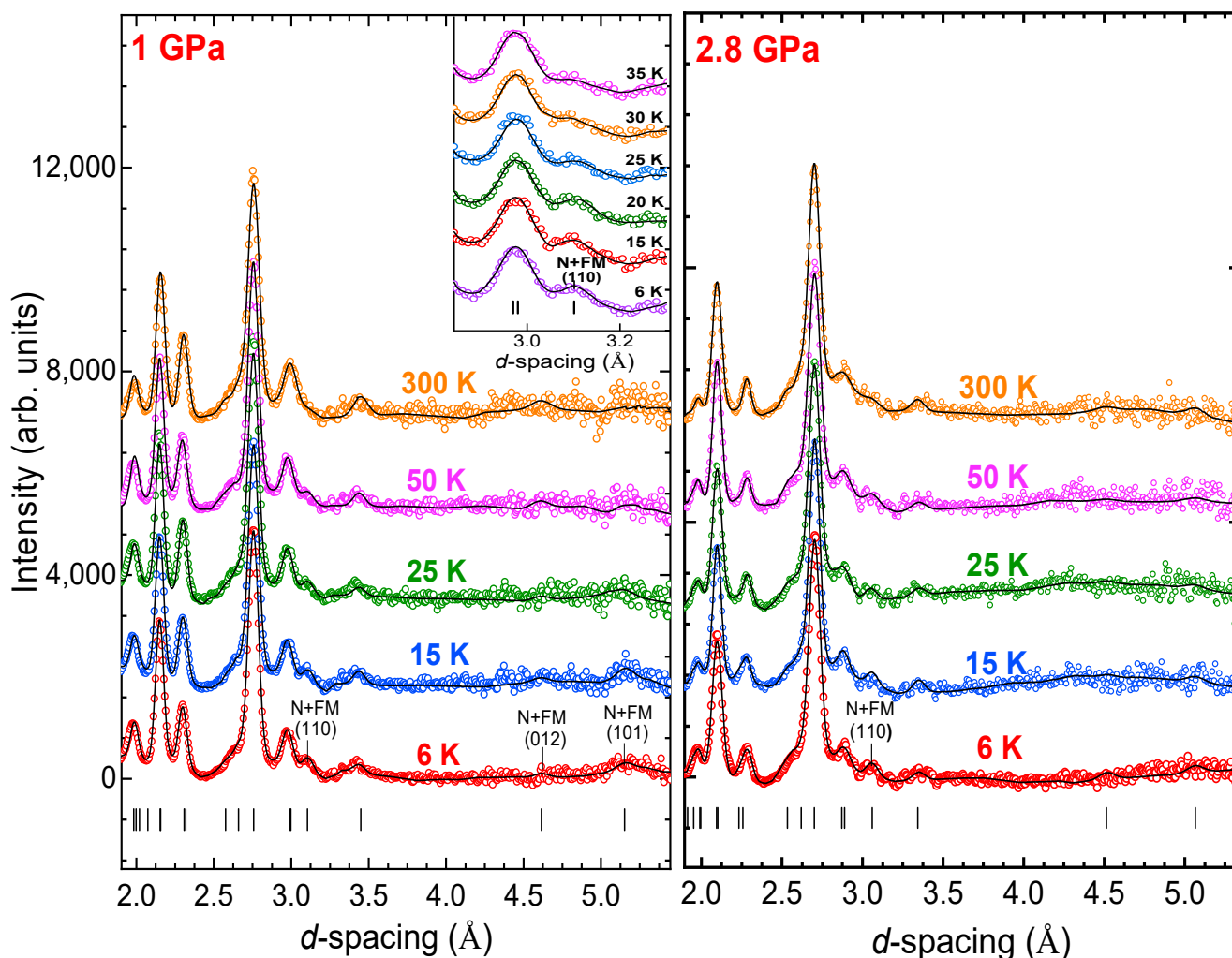


Figure 2. Neutron diffraction patterns of CrBr_3 measured at selected pressures and temperatures and refined by the Rietveld method. The experimental points and calculated profiles are shown. Ticks below represent calculated positions of the nuclear peaks of the rhombohedral phase of CrBr_3 . The magnetic contribution into nuclear peaks is labeled as “N+FM”. Inset: the pressure evolution of the characteristic peak with additional magnetic contribution.

The extrapolation of the experimental Curie temperature pressure dependence of our work showed (Figure 3c) that the T_C value turned to zero at $P_C \sim 8.4$ GPa. Therefore, one might expect a modification of the ground state in CrBr_3 from FM to either AFM or a magnetically disordered state in the high-pressure phase for $P > P_C$. The pressure evolution of magnetic exchange coupling constants in CrBr_3 was theoretically studied by means of *ab-initio* calculations [37]. It was revealed that in a wide pressure range, the in-plane exchange constant J_{in} for CrBr_3 took a dominant value compared to the out-of-plane J_{out} , and it decreased rapidly. In contrast, a weak growth of J_{out} occurred under pressure. The pronounced pressure-induced reduction of the J_{in} exchange constant was a possible mechanism for a destabilization of the FM ground state in CrBr_3 . It also followed an evolution trend from the FM to AFM state upon the “chemical” pressure effect in the CrY_3 family by halide ionic radius (and relevant lattice volume) reduction from I to Cl.

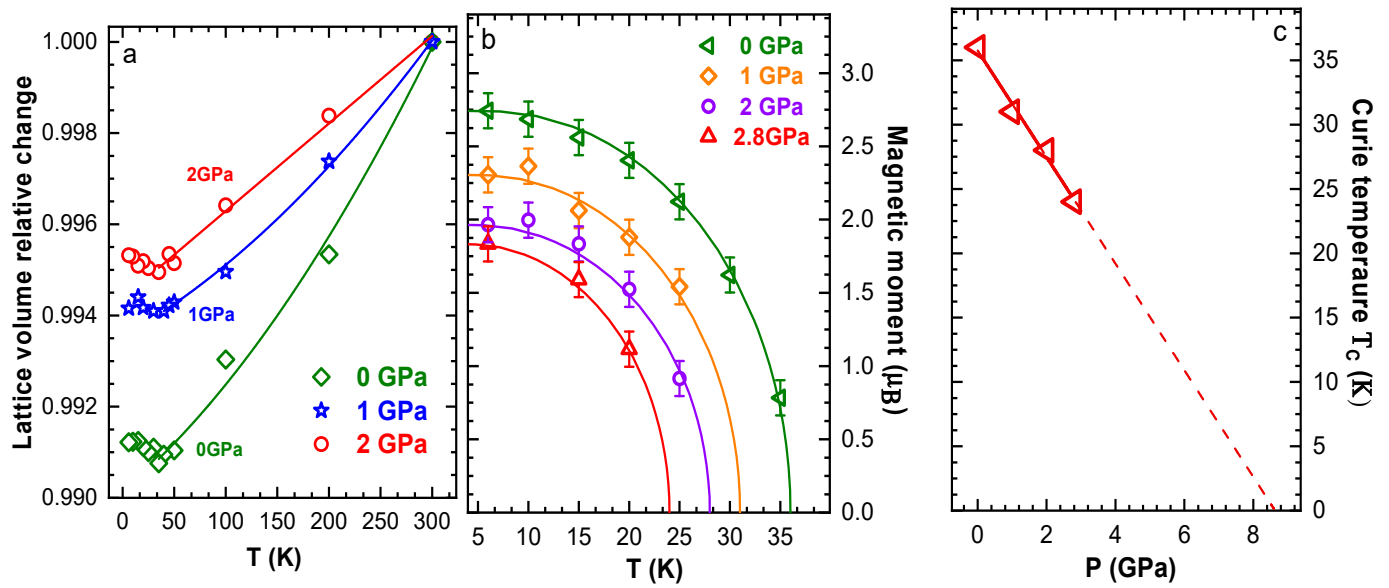


Figure 3. (a) The temperature dependences of the unit-cell volume obtained from neutron diffraction and normalized to the ambient temperature values; (b) The temperature dependences of the ordered Cr³⁺ magnetic moments at selected pressures. The solid lines represent fitting by function described by Equation (2); (c) Curie temperature as a function of pressure and its linear extrapolation.

3.3. Raman Spectroscopy

The Raman spectra of CrBr₃ measured at various pressures up to ~22 GPa are shown in Figure 4. At pressures below 2.5 GPa, six Raman active modes were observed, in consistency with the rhombohedral R $\bar{3}$ lattice symmetry [26,38–40]. They were assigned as 73.4 cm⁻¹ (E_g^1), 106 cm⁻¹ (A_g^1), 141.2 cm⁻¹ (E_g^2), 149.6 cm⁻¹ (E_g^3), 184.8 cm⁻¹ (A_g^2), 279.5 cm⁻¹ (E_g^4) (Table 1). According to [40], the A_g^1 and A_g^2 modes were mainly associated with in-plane and out-of-plane vibrations of Br atoms, respectively. It was demonstrated that the E_g^3 and E_g^2 modes were degenerate, resembling the in-plane shear motion of the Br atomic planes and also involving Cr atoms with out-of-plane displacements [40]. The pressure coefficients and calculated Gruneisen parameters γ for all the observed Raman modes are listed in Table 1.

Table 1. The assignment and frequencies of Raman mode, the pressure coefficients and mode Gruneisen parameters γ_i for vibration modes of CrBr₃ calculated for different pressure ranges. The mode Gruneisen parameters γ_i are determined as $\gamma_i = B_0/v_i(dv_i/dP)_T$, where B_0 is the bulk modulus ($B_0 = 23(4)$ GPa for $P < 6$ GPa and $B_0 = 94(4)$ GPa for $P > 6$ GPa).

Mode Symmetry	ν_0 (cm ⁻¹)	dv_i/dP (cm ⁻¹ /GPa)	γ_i
E_g^1	73.4	2.27 ($P < 6$ GPa) 1.23 ($P > 6$ GPa)	0.71 ($P < 6$ GPa) 1.45 ($P > 6$ GPa)
A_g^1	106.05	4.0 ($P < 6$ GPa) 1.22 ($P > 6$ GPa)	0.87 ($P < 6$ GPa) 0.96 ($P > 6$ GPa)
M_1	116.08	2.82	2.29
E_g^2	142.18	1.33	0.22
E_g^3	149.6	2.64	0.4
A_g^2	184.8	3.57	0.44
E_g^4	279.56	3.39	0.27

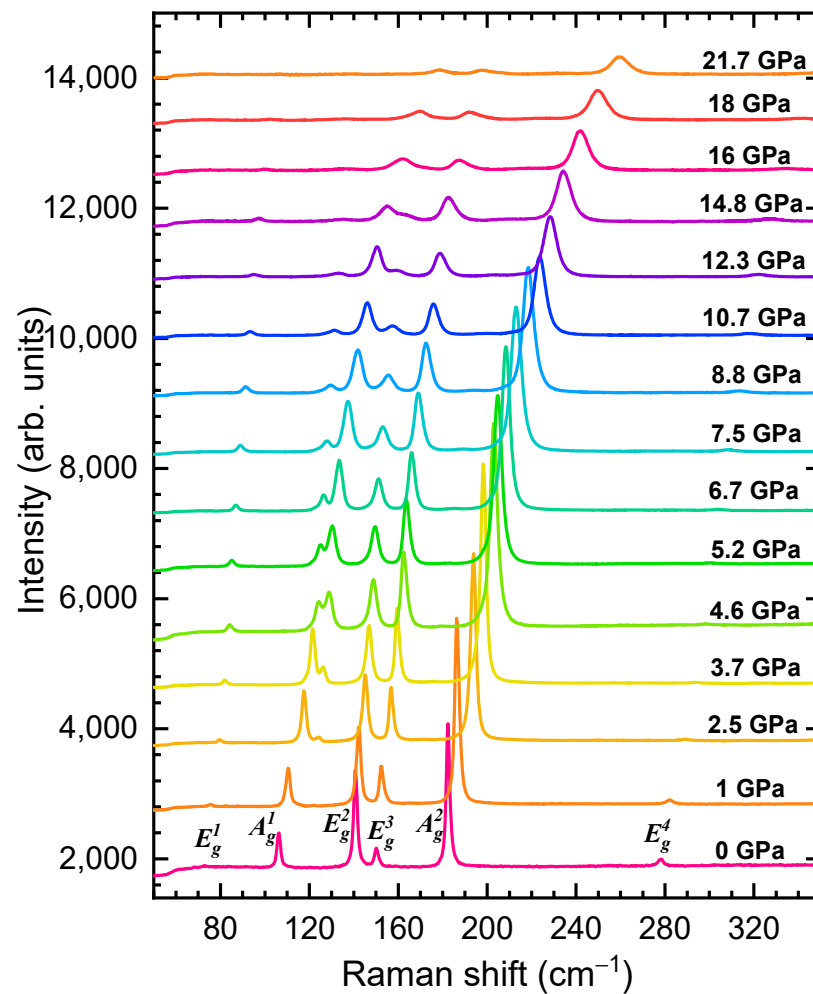


Figure 4. The Raman spectra of CrBr₃ measured at selected pressures and room temperature.

At pressures above 2.5 GPa, the emergence of a new Raman mode was observed at 116.08 cm⁻¹, further labeled as M₁. Upon further compression, intensities of this mode and the E_g³ one increased strongly, while the intensity of the A_g¹ mode rapidly suppressed (Figure 4). At P ~15 GPa, the E_g² mode merged with M₁. Above this pressure, noticeable broadening of the Raman lines was found.

Most of the observed Raman mode frequencies, except for A_g¹ and E_g¹, increased nearly linearly under pressure (Figure 5). The pressure dependence of the A_g¹ mode demonstrated a sharp change of the pressure coefficient at P~6 GPa, correlating with the anomaly in the pressure behavior of the c lattice parameter (Figure 2c). A similar less pronounced change also occurred for the E_g¹ mode. These effects, along with observation of the M₁ mode, were associated with the gradual isostructural phase transition, which likely started at P~2.5 GPa and evolved up to 7 GPa, becoming first visible in the Raman spectra and, subsequently, in the XRD patterns, when sufficient volume of the material was being transformed. The merging of the E_g² and M₁ modes, along with another weaker modification of the A_g¹ mode pressure coefficient at 15 GPa (Figure 5), might be a signature of another phase transition. Taking into account the absence of qualitative changes in the XRD patterns, this transformation might be of an electronic nature, like the semiconductor to metal transition observed in CrI₃ at pressures above 22 GPa [23] and in CrCl₃ at ~30 GPa [24].

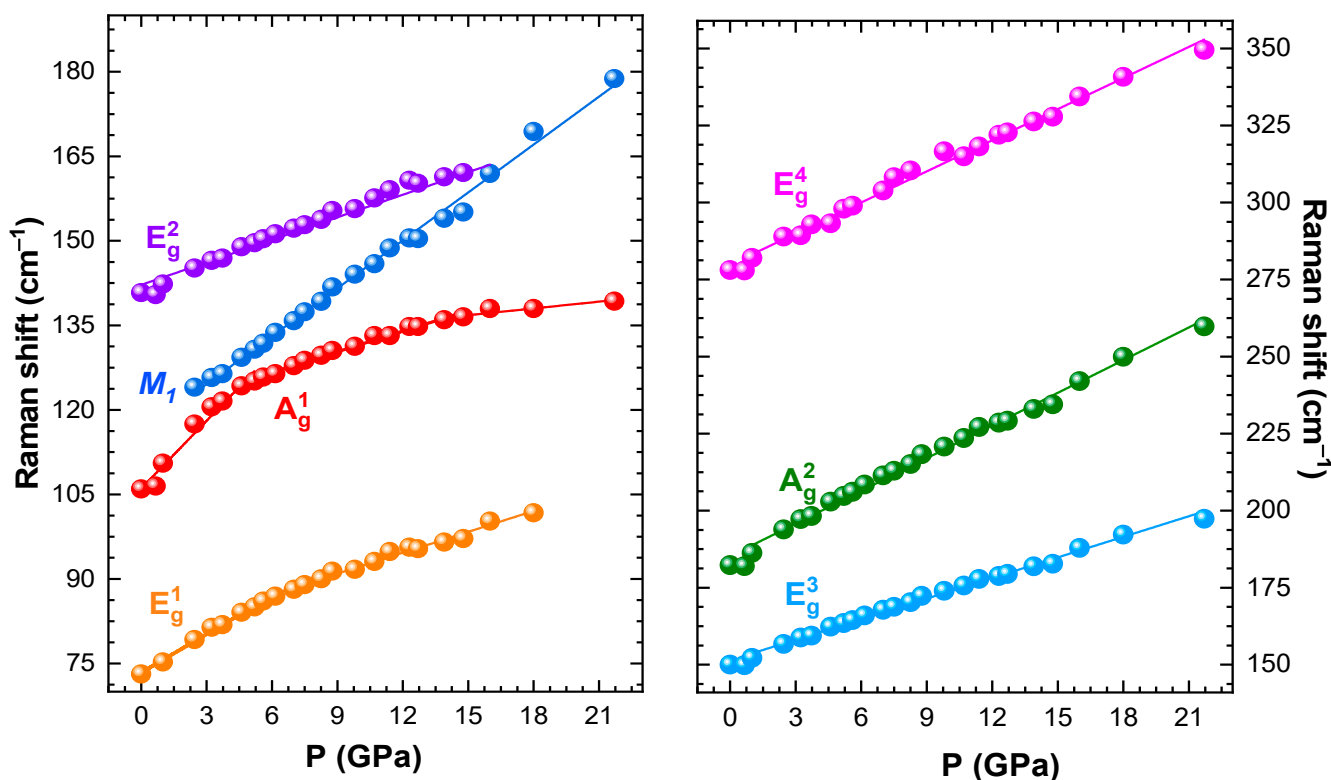


Figure 5. Pressure dependences of selected Raman shift for CrBr₃. Solid lines are linear fits to the observed frequencies.

4. Conclusions

Our results demonstrated that the pressure-induced isostructural phase transition evolved gradually in vdW ferromagnet CrBr₃ over a pressure range of 2.5–7 GPa. This transition emerged in Raman spectra around $P \sim 2.5$ GPa by the appearance of an extra Raman mode and manifested finally in anomalies in the pressure behavior of the lattice parameters, unit cell volume, and A_g^1 and E_g^1 vibrational mode frequencies at $P \sim 6$ –7 GPa, when a volume of the pressure-induced phase became sufficiently dominant. The Curie temperature of CrBr₃ reduced rapidly with a pressure coefficient $dT_C/dP = -4.1(4)$ K/GPa, implying instability of the initial FM order. A full suppression of the FM state and a magnetic transition to either AFM state or into a magnetically disordered one was expected at $P \sim 8.4$ GPa. Additional anomalies in pressure behavior of Raman mode frequencies, detected at $P \sim 15$ GPa, pointed to another phase transformation, presumably associated with the metallization process.

Author Contributions: D.K., S.K., E.L., I.Z. and B.S. performed the neutron diffraction experiments and data analysis. O.L., I.Z. and E.L. performed the X-ray diffraction and Raman spectroscopy experiments and data analysis. O.L., D.K. and S.K. prepared the first draft of manuscript and all authors contribute to the final version of the manuscript. All authors have read and agreed to the published version of the manuscript.

Funding: This research did not receive any specific grant from funding agencies in the public, commercial, or not-for-profit sectors.

Institutional Review Board Statement: Not applicable.

Informed Consent Statement: Not applicable.

Data Availability Statement: Not applicable.

Conflicts of Interest: The authors declare no conflict of interest.

References

1. Gong, C.; Li, L.; Li, Z.; Ji, H.; Stern, A.; Xia, Y.; Cao, T.; Bao, W.; Wang, C.; Wang, Y.; et al. Discovery of Intrinsic Ferromagnetism in Two-Dimensional van Der Waals Crystals. *Nature* **2017**, *546*, 265–269. [[CrossRef](#)] [[PubMed](#)]
2. Huang, B.; Clark, G.; Navarro-Moratalla, E.; Klein, D.R.; Cheng, R.; Seyler, K.L.; Zhong, D.; Schmidgall, E.; McGuire, M.A.; Cobden, D.H.; et al. Layer-Dependent Ferromagnetism in a van Der Waals Crystal down to the Monolayer Limit. *Nature* **2017**, *546*, 270–273. [[CrossRef](#)] [[PubMed](#)]
3. Burch, K.S.; Mandrus, D.; Park, J.G. Magnetism in Two-Dimensional van Der Waals Materials. *Nature* **2018**, *563*, 47–52. [[CrossRef](#)]
4. Zhang, W.; Wong, P.K.J.; Zhu, R.; Wee, A.T.S. Van Der Waals Magnets: Wonder Building Blocks for Two-Dimensional Spintronics? *InfoMat* **2019**, *1*, 479–495. [[CrossRef](#)]
5. Wang, M.C.; Huang, C.C.; Cheung, C.H.; Chen, C.Y.; Tan, S.G.; Huang, T.W.; Zhao, Y.; Zhao, Y.; Wu, G.; Feng, Y.P.; et al. Prospects and Opportunities of 2D van Der Waals Magnetic Systems. *Ann. Phys.* **2020**, *532*, 1900452. [[CrossRef](#)]
6. Zhang, W.B.; Qu, Q.; Zhu, P.; Lam, C.H. Robust Intrinsic Ferromagnetism and Half Semiconductivity in Stable Two-Dimensional Single-Layer Chromium Trihalides. *J. Mater. Chem. C* **2015**, *3*, 12457–12468. [[CrossRef](#)]
7. Novoselov, K.S.; Mishchenko, A.; Carvalho, A.; Castro Neto, A.H. 2D Materials and van Der Waals Heterostructures. *Science* **2016**, *353*, aac9439. [[CrossRef](#)]
8. Soriano, D.; Katsnelson, M.I.; Fernández-Rossier, J. Magnetic Two-Dimensional Chromium Trihalides: A Theoretical Perspective. *Nano Lett.* **2020**, *20*, 6225–6234. [[CrossRef](#)]
9. Song, T.; Fei, Z.; Yankowitz, M.; Lin, Z.; Jiang, Q.; Hwangbo, K.; Zhang, Q.; Sun, B.; Taniguchi, T.; Watanabe, K.; et al. Switching 2D Magnetic States via Pressure Tuning of Layer Stacking. *Nat. Mater.* **2019**, *18*, 1298–1302. [[CrossRef](#)]
10. Li, T.; Jiang, S.; Sivadas, N.; Wang, Z.; Xu, Y.; Weber, D.; Goldberger, J.E.; Watanabe, K.; Taniguchi, T.; Fennie, C.J.; et al. Pressure-Controlled Interlayer Magnetism in Atomically Thin CrI₃. *Nat. Mater.* **2019**, *18*, 1303–1308. [[CrossRef](#)]
11. Xu, C.; Wang, Q.J.; Xu, B.; Hu, J. Effect of Biaxial Strain and Hydrostatic Pressure on the Magnetic Properties of Bilayer CrI₃. *Front. Phys.* **2021**, *16*, 53502. [[CrossRef](#)]
12. Haines, C.R.S.; Coak, M.J.; Wildes, A.R.; Lampronti, G.I.; Liu, C.; Nahai-Williamson, P.; Hamidov, H.; Daisenberger, D.; Saxena, S.S. Pressure-Induced Electronic and Structural Phase Evolution in the van Der Waals Compound FePS₃. *Phys. Rev. Lett.* **2018**, *121*, 266801. [[CrossRef](#)] [[PubMed](#)]
13. Das, S.; Chaturvedi, S.; Tripathy, D.; Grover, S.; Singh, R.; Muthu, D.V.S.; Sampath, S.; Waghmare, U.V.; Sood, A.K. Raman and First-Principles Study of the Pressure-Induced Mott-Insulator to Metal Transition in Bulk FePS₃. *J. Phys. Chem. Solids* **2022**, *164*, 110607. [[CrossRef](#)]
14. Wang, Y.; Ying, J.; Zhou, Z.; Sun, J.; Wen, T.; Zhou, Y.; Li, N.; Zhang, Q.; Han, F.; Xiao, Y.; et al. Emergent Superconductivity in an Iron-Based Honeycomb Lattice Initiated by Pressure-Driven Spin-Crossover. *Nat. Commun.* **2018**, *9*, 1914. [[CrossRef](#)]
15. Coak, M.J.; Jarvis, D.M.; Hamidov, H.; Wildes, A.R.; Paddison, J.A.M.; Liu, C.; Haines, C.R.S.; Dang, N.T.; Kichanov, S.E.; Savenko, B.N.; et al. Emergent Magnetic Phases in Pressure-Tuned van Der Waals Antiferromagnet FePS₃. *Phys. Rev. X* **2021**, *11*, 11024. [[CrossRef](#)]
16. Cai, W.; Sun, H.; Xia, W.; Wu, C.; Liu, Y.; Liu, H.; Gong, Y.; Yao, D.X.; Guo, Y.; Wang, M. Pressure-Induced Superconductivity and Structural Transition in Ferromagnetic CrSiTe₃. *Phys. Rev. B* **2020**, *102*, 144525. [[CrossRef](#)]
17. Lin, Z.; Lohmann, M.; Ali, Z.A.; Tang, C.; Li, J.; Xing, W.; Zhong, J.; Jia, S.; Han, W.; Coh, S.; et al. Pressure-Induced Spin Reorientation Transition in Layered Ferromagnetic Insulator Cr₂Ge₂Te₆. *Phys. Rev. Mater.* **2018**, *2*, 051004. [[CrossRef](#)]
18. Mondal, S.; Kannan, M.; Das, M.; Govindaraj, L.; Singha, R.; Satpati, B.; Arumugam, S.; Mandal, P. Effect of Hydrostatic Pressure on Ferromagnetism in Two-Dimensional CrI₃. *Phys. Rev. B* **2019**, *99*, 180407. [[CrossRef](#)]
19. Valenta, J.; Kratochvílová, M.; Míšek, M.; Carva, K.; Kaštil, J.; Doležal, P.; Opletal, P.; Čermák, P.; Proschek, P.; Uhlířová, K.; et al. Pressure-Induced Large Increase of Curie Temperature of the van Der Waals Ferromagnet VI₃. *Phys. Rev. B* **2021**, *103*, 054424. [[CrossRef](#)]
20. Sun, Y.; Xiao, R.C.; Lin, G.T.; Zhang, R.R.; Ling, L.S.; Ma, Z.W.; Luo, X.; Lu, W.J.; Sun, Y.P.; Sheng, Z.G. Effects of Hydrostatic Pressure on Spin-Lattice Coupling in Two-Dimensional Ferromagnetic Cr₂Ge₂Te₆. *Appl. Phys. Lett.* **2018**, *112*, 072409. [[CrossRef](#)]
21. Yoshida, H.; Chiba, J.; Kaneko, T.; Fujimori, Y.; Abe, S. Pressure Effect on the Curie Temperature of CrBr₃. *Phys. B Condens. Matter* **1997**, *237–238*, 525–526. [[CrossRef](#)]
22. Ding, S.; Liang, Z.; Yang, J.; Yun, C.; Zhang, P.; Li, Z.; Xue, M.; Liu, Z.; Tian, G.; Liu, F.; et al. Ferromagnetism in Two-Dimensional Fe₃GeTe₂; Tunability by Hydrostatic Pressure. *Phys. Rev. B* **2021**, *103*, 94429. [[CrossRef](#)]
23. Ghosh, A.; Singh, D.; Aramaki, T.; Mu, Q.; Borisov, V.; Kvashnin, Y.; Haider, G.; Jonak, M.; Chareev, D.; Medvedev, S.A.; et al. Exotic Magnetic and Electronic Properties of Layered Formula Presented Single Crystals under High Pressure. *Phys. Rev. B* **2022**, *105*, L081104. [[CrossRef](#)]
24. Hong, M.; Dai, L.; Hu, H.; Zhang, X.; Li, C.; He, Y. Pressure-Induced Structural Phase Transition and Metallization of CrCl₃ under Different Hydrostatic Environments up to 50.0 GPa. *Inorg. Chem.* **2022**, *61*, 4852–4864. [[CrossRef](#)]
25. Ahmad, A.S.; Liang, Y.; Dong, M.; Zhou, X.; Fang, L.; Xia, Y.; Dai, J.; Yan, X.; Yu, X.; Dai, J.; et al. Pressure-Driven Switching of Magnetism in Layered CrCl₃. *Nanoscale* **2020**, *12*, 22935–22944. [[CrossRef](#)]
26. Kozlenko, D.P.; Lis, O.N.; Kichanov, S.E.; Lukin, E.V.; Belozerova, N.M.; Savenko, B.N. Spin-Induced Negative Thermal Expansion and Spin-Phonon Coupling in van Der Waals Material CrBr₃. *Npj. Quantum Mater.* **2021**, *6*, 19. [[CrossRef](#)]

27. Wu, J.; Yao, Y.; Lin, M.L.; Rösner, M.; Du, Z.; Watanabe, K.; Taniguchi, T.; Tan, P.H.; Haas, S.; Wang, H. Spin–Phonon Coupling in Ferromagnetic Monolayer Chromium Tribromide. *Adv. Mater.* **2022**, *34*, e2108506. [[CrossRef](#)]
28. Liu, S.; Long, M.Q.; Wang, Y.P. Negative Thermal Expansion of Two-Dimensional Magnets. *Appl. Phys. Lett.* **2022**, *120*, 072403. [[CrossRef](#)]
29. Kozlenko, D.; Kichanov, S.; Lukin, E.; Savenko, B. The DN-6 Neutron Diffractometer for High-Pressure Research at Half a Megabar Scale. *Crystals* **2018**, *8*, 331. [[CrossRef](#)]
30. Kozlenko, D.P.; Kichanov, S.E.; Lukin, E.V.; Savenko, B.N. High-Pressure Neutron Diffraction Study of the Crystal and Magnetic Structure of Materials at the Pulsed Reactor IBR-2: Current Opportunities and Prospects. *Crystallogr. Rep.* **2021**, *66*, 303–313. [[CrossRef](#)]
31. Rodríguez-Carvajal, J. Recent Advances in Magnetic Structure Determination by Neutron Powder Diffraction. *Phys. B Phys. Condens. Matter* **1993**, *192*, 55–69. [[CrossRef](#)]
32. Olmos, R.; Alam, S.; Chang, P.H.; Gandha, K.; Nlebedim, I.C.; Cole, A.; Tafti, F.; Zope, R.R.; Singamaneni, S.R. Pressure Dependent Magnetic Properties on Bulk CrBr₃ Single Crystals. *J. Alloys Compd.* **2022**, *911*, 165034. [[CrossRef](#)]
33. Yu, Z.; Xia, W.; Xu, K.; Xu, M.; Wang, H.; Wang, X.; Yu, N.; Zou, Z.; Zhao, J.; Wang, L.; et al. Pressure-Induced Structural Phase Transition and a Special Amorphization Phase of Two-Dimensional Ferromagnetic Semiconductor Cr₂Ge₂Te₆. *J. Phys. Chem. C* **2019**, *123*, 13885–13891. [[CrossRef](#)]
34. Xu, K.; Yu, Z.; Xia, W.; Xu, M.; Mai, X.; Wang, L.; Guo, Y.; Miao, X.; Xu, M. Unique 2D-3D Structure Transformations in Trichalcogenide CrSiTe₃ under High Pressure. *J. Phys. Chem. C* **2020**, *124*, 15600–15606. [[CrossRef](#)]
35. Birch, F. Equation of State and Thermodynamic Parameters of NaCl to 300 Kbar in the High-Temperature Domain. *J. Geophys. Res.* **1986**, *91*, 4949. [[CrossRef](#)]
36. Cai, W.; Yan, L.; Chong, S.K.; Xu, J.; Zhang, D.; Deshpande, V.V.; Zhou, L.; Deemyad, S. Pressure-Induced Metallization in the Absence of a Structural Transition in the Layered Ferromagnetic Insulator Cr₂Ge₂Te₆. *Phys. Rev. B* **2022**, *106*, 085116. [[CrossRef](#)]
37. Fumega, A.O.; Blanco-Canosa, S.; Babu-Vasili, H.; Gargiani, P.; Li, H.; Zhou, J.S.; Rivadulla, F.; Pardo, V. Electronic Structure and Magnetic Exchange Interactions of Cr-Based van Der Waals Ferromagnets. A Comparative Study between CrBr₃ and Cr₂Ge₂Te₆. *J. Mater. Chem. C* **2020**, *8*, 13582–13589. [[CrossRef](#)]
38. Bermudezt, V.M. Unit-cell vibrational spectra of chromium trichloride and chromium tribromide. *Solid State Commun.* **1976**, *19*, 693–697. [[CrossRef](#)]
39. Larson, D.T.; Kaxiras, E. Raman Spectrum of CrI₃: An Ab Initio Study. *Phys. Rev. B* **2018**, *98*, 2–6. [[CrossRef](#)]
40. Yin, T.; Ulman, K.A.; Liu, S.; Granados del Águila, A.; Huang, Y.; Zhang, L.; Serra, M.; Sedmidubsky, D.; Sofer, Z.; Quek, S.Y.; et al. Chiral Phonons and Giant Magneto-Optical Effect in CrBr₃ 2D Magnet. *Adv. Mater.* **2021**, *33*, 2101618. [[CrossRef](#)]

Disclaimer/Publisher’s Note: The statements, opinions and data contained in all publications are solely those of the individual author(s) and contributor(s) and not of MDPI and/or the editor(s). MDPI and/or the editor(s) disclaim responsibility for any injury to people or property resulting from any ideas, methods, instructions or products referred to in the content.